

# Metalorganic Polyhedra Polyoxometalate Hybrid Salts for Tandem Photooxidative-Hydrolytic Pesticide Detoxification

Cristina Perona-Bermejo, Rebecca Vismara, Natalia M. Padial, Neyvis Almora-Barrios, Carmen R. Maldonado, Teresa J. Bandosz, Pablo Garrido-Barros, Francisco J. Carmona,\* and Jorge A. R. Navarro\*

The extensive use of pesticides to ensure global food production presents significant threats to both human health and the environment. In this study, the photochemical, redox, and acid-base properties of Zr-metal-organic polyhedra (Zr-MOP) and polyoxometalates (POM) are utilized to fabricate functional hybrid salts, denoted as [Zr-MOP][POM], designed for pesticide detoxification. Upon light irradiation, [Zr-MOP][POM] salts generate a charge-separated state with oxidizing properties. This activated state selectively photooxidizes highly toxic and persistent fenamiphos into fenamiphos sulfoxide and subsequently hydrolytically breaks down it into non-toxic 3-methyl-4-(methylsulfinyl)phenol and phosphate components. The hydrolytic degradation of fenamiphos is facilitated by the reduced basicity of the 3-methyl-4-(methylsulfinyl)phenolate residue ( $\Delta pK_b = -2.4$ ) in the photooxidized form of the pesticide molecule. Furthermore, the hybrid salts demonstrate efficacy in the breakdown of multicomponent pesticide mixtures such as fenamiphos and methylparaoxon.

## 1. Introduction

The widespread use of pesticides in global food production presents significant hazards to human health and the environment, contributing to  $\approx 110\,000$  deaths annually and causing  $\approx 385$  million cases of unintentional acute pesticide poisoning.<sup>[1,2]</sup> Of particular concern are highly persistent organophosphate (OP) pollutants, of which fenamiphos (Fen) serves as a notable example (Scheme 1). Fen is characterized by its high toxicity (LD<sub>50</sub> oral rats of 2.5 mg kg<sup>-1</sup>, classified as Toxicity Category I). Moreover, it exhibits a hydrolysis half-life exceeding 234 days in anaerobic groundwater, underscoring its enduring presence and potential for environmental and health damage.<sup>[3]</sup>

Polyoxometalates (POM), such as certain niobate, molybdate, or tungstate POMs, have been proven to display good hydrolytic activity toward phosphoester bonds thanks to the Lewis acidity of their metal centers.<sup>[4–8]</sup> POMs have also been

proposed as catalysts in the photo-driven oxidation of a wide range of substrates by exploiting their tunable (photo)redox properties.<sup>[9]</sup> On the other hand, metal-organic framework materials (MOFs) have been exploited for pesticide capture and degradation due to their high porosity and synthetic tunability.<sup>[10]</sup> Among them, Zr-MOFs<sup>[11,12]</sup> and their molecular counterparts Zr-metal-organic polyhedra (Zr-MOPs)<sup>[13,14]</sup> have been shown to be useful for the capture and hydrolytic degradation of OP compounds. However, they usually need the use of strong basic/toxic amine molecules to boost their hydrolytic activity.<sup>[15]</sup> Alternatively, photocatalytic generation of highly reactive oxygen-based species, such as OH· and <sup>1</sup>O<sub>2</sub>, for the degradation of toxic molecules, has also been explored using porphyrin-based MOF systems.<sup>[16]</sup> It should be noted that such a photooxidative approach lacks selectivity and can be detrimental to the stability of the metal-organic catalyst itself. Therefore, the degradation of persistent toxic molecules, under mild and environmentally relevant conditions, remains a major challenge.

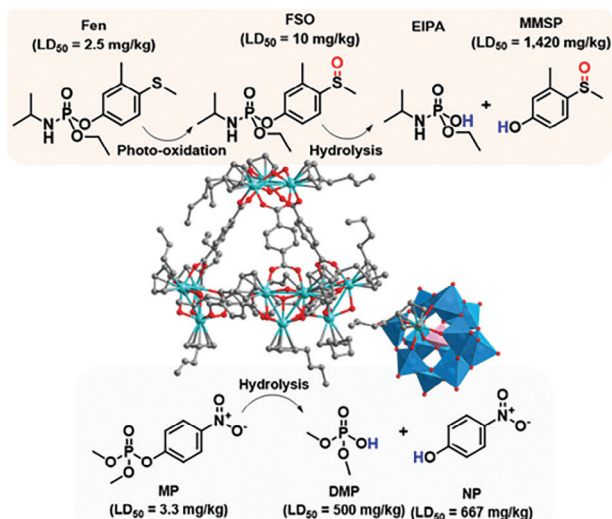
In this study, we have investigated the potential synergistic effects arising from the combined photochemical, acid-base, and redox properties inherent in hybrid salts composed of zirconium-metal-organic polyhedra (Zr-MOP) and polyoxometalates (POM)

C. Perona-Bermejo, R. Vismara, C. R. Maldonado, P. Garrido-Barros, F. J. Carmona, J. A. R. Navarro  
Departamento de Química Inorgánica  
Universidad de Granada  
Av. Fuentenueva S/N, Granada 18071, Spain  
E-mail: [fjcarmona@ugr.es](mailto:fjcarmona@ugr.es); [jarn@ugr.es](mailto:jarn@ugr.es)  
N. M. Padial, N. Almora-Barrios  
Functional Inorganic Materials Team  
Instituto de Ciencia Molecular (ICMol)  
Universitat de València  
Calle Catedrático José Beltrán Martínez, 2, Paterna, Valencia 46980, Spain  
T. J. Bandosz  
Department of Chemistry  
The City University of New York (CUNY)  
160 Convent Avenue, New York, NY 10031, USA

The ORCID identification number(s) for the author(s) of this article can be found under <https://doi.org/10.1002/adfm.202405785>

© 2024 The Author(s). Advanced Functional Materials published by Wiley-VCH GmbH. This is an open access article under the terms of the Creative Commons Attribution-NonCommercial-NoDerivs License, which permits use and distribution in any medium, provided the original work is properly cited, the use is non-commercial and no modifications or adaptations are made.

DOI: 10.1002/adfm.202405785



**Scheme 1.** Tandem photooxidative-hydrolytic degradation of fenamiphos (Fen) and hydrolytic degradation of methylparaoxon (MP) by hybrid  $[\text{Zr-MOP}][\text{ZrCp}_W\text{-POM}]$  salt.

for the detoxification of persistent pesticides. To validate the advantageous integration of the properties of both components within a hybrid salt matrix, we demonstrate their ability to facilitate the sequential photooxidative and hydrolytic degradation of the persistent Fen pollutant, as shown in Scheme 1. Furthermore, we extend this detoxification efficacy to the simultaneous detoxification of Fen and methylparaoxon (MP) ( $\text{LD}_{50}$  oral rat of  $3.3 \text{ mg kg}^{-1}$ ) during three catalytic cycles.

## 2. Results and Discussion

Synthesis and structural characterization of  $[\text{Zr-MOP}][\text{M-POM}]$  hybrid salts ( $\text{M} = \text{Mo}$  or  $\text{W}$ )

$[\text{((n-butylCpZr)}_3(\text{O}_4\text{H}_{3.75}))_4(\text{benzene-1,4-dicarboxylate})_6][\text{PMo}_{12}\text{O}_{40}]\text{Cl}_3$   $[\text{Zr-MOP}][\text{Mo-POM}]$  and  $[\text{((n-butylCpZr)}_3(\text{O}_4\text{H}_{3.5}))_4(\text{benzene-1,4-dicarboxylate})_6][\text{n-butylCpZrPW}_{11}\text{O}_{39}]\text{Cl}_2$   $[\text{Zr-MOP}][\text{ZrCp}_W\text{-POM}]$  hybrid salts were prepared by mixing two equimolecular methanolic solutions of  $[\text{((n-butylCpZr)}_3(\text{O}_4\text{H}_{3.5}))_4(\text{benzene-1,4-dicarboxylate})_6]\text{Cl}_6$ <sup>[13]</sup>, and  $\text{H}_3[\text{PM}_{12}\text{O}_{40}]$  ( $\text{M} = \text{Mo}$ ,  $\text{W}$ ).

The structure of  $[\text{Zr-MOP}][\text{Mo-POM}]$  and  $[\text{Zr-MOP}][\text{ZrCp}_W\text{-POM}]$  hybrid salts have been univocally established by single crystal X-ray diffraction (Figure 1; Figures S1 and S2 and Table S1, Supporting Information). Both salts have a MOP:POM 1:1 stoichiometry but are chemically and structurally different. On one hand,  $[\text{Zr-MOP}][\text{Mo-POM}]$  crystallizes in the monoclinic space group  $\text{C2/c}$  with unit cell parameters:  $a = 48.4090(4) \text{ \AA}$ ,  $b = 43.7993(4) \text{ \AA}$ ,  $c = 31.0080(2) \text{ \AA}$ ,  $\beta = 97.7940(10)^\circ$  and  $V = 65138.3 \text{ \AA}^3$ .  $[\text{Zr-MOP}][\text{Mo-POM}]$  crystal structure is built of  $[\text{((n-butylCpZr)}_3(\text{O}_4\text{H}_{3.5}))_4(\text{benzene-1,4-dicarboxylate})_6]^{6+}$  tetrahedral cationic cages with inner voids of  $\approx 490 \text{ \AA}^3$  and  $[\text{PMo}_{12}\text{O}_{40}]^{3-}$  polyoxometalate and three chloride anions. *N,N*-dimethylacetamide (DMA) molecules fill the space between the Zr-MOP and Mo-POM counterions (5–6  $\text{ \AA}$  wide channels) with their main role being to solvate the Mo-POM anions. This structure can be related to the previously re-

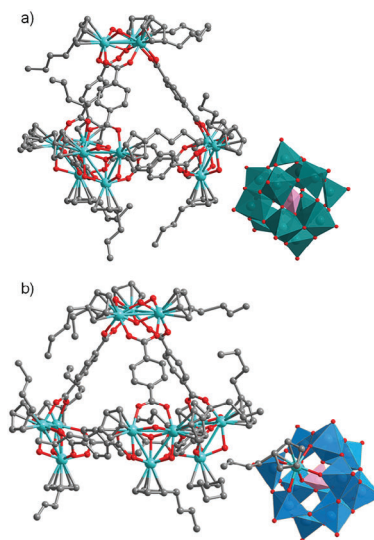


**Figure 1.** Structures of a)  $[\text{Zr-MOP}][\text{Mo-POM}]$  and b)  $[\text{Zr-MOP}][\text{ZrCp}_W\text{-POM}]$  hybrid salts. H and Cl atoms have been omitted for sake of clarity. Color code: Zr (cyan), Mo (olive), W (blue), C (grey), O (red), P (pink).

ported  $[\text{((CpZr)}_3\text{O}_4\text{H}_3)_4(\text{L})_6][\text{SiM}_{12}\text{O}_{40}]$  systems in which the formation of the hybrid salts enhanced their component's stability.<sup>[17]</sup> On the other hand,  $[\text{Zr-MOP}][\text{ZrCp}_W\text{-POM}]$  crystallizes in the triclinic space group  $P-1$  with unit cell parameters:  $a = 22.7488(10) \text{ \AA}$ ,  $b = 23.8088(10) \text{ \AA}$ ,  $c = 28.4398(13) \text{ \AA}$ ,  $\alpha = 108.3514(13)^\circ$ ,  $\beta = 101.3959(14)^\circ$ ,  $\gamma = 101.8264(13)^\circ$  and  $V = 13728.5 \text{ \AA}^3$ .  $[\text{Zr-MOP}][\text{ZrCp}_W\text{-POM}]$  crystal structure contains  $[\text{((n-butylCpZr)}_3(\text{O}_4\text{H}_{3.5}))_4(\text{benzene-1,4-dicarboxylate})_6]^{6+}$  tetrahedral cationic cages, and  $[\text{n-butylCpZrPW}_{11}\text{O}_{39}]^{4-}$  polyoxometalate and two chloride anions. The crystal structure packing is stabilized by close 2.69  $\text{ \AA}$  H-bonding interactions between the bridging hydroxide group of the  $[\text{Zr-MOP}]$  and apical oxygen atoms of the  $[\text{ZrCp}_W\text{-POM}]$  counterions. Additional contacts of 3.6  $\text{ \AA}$  are established between the Cp residue of  $[\text{ZrCp}_W\text{-POM}]$  and the benzene ring of terephthalate linkers in  $[\text{Zr-MOP}]$ . The formation of the heterometallic Zr–W polyoxometalate,  $[\text{n-butylCpZrPW}_{11}\text{O}_{39}]^{4-}$ , was unexpected, but is in agreement with previous reports on the tendency to form heterometallic Zr–W polyoxometallates as found for dimeric  $(\text{Et}_2\text{NH}_2)_8[\{\alpha\text{-PW}_{11}\text{O}_{39}\text{Zr}(\mu\text{-OH})(\text{H}_2\text{O})\}_2] \cdot 7\text{H}_2\text{O}$  ( $\text{Zr}_W\text{-POM}$ ) polyoxometalate.<sup>[18]</sup> The exchange of one W atom in  $[\text{PW}_{12}\text{O}_{40}]^{3-}$  by *n*-butylCpZr residue to give rise to heterometallic  $[\text{n-butylCpZrPW}_{11}\text{O}_{39}]^{4-}$   $[\text{ZrCp}_W\text{-POM}]$  is highly favored since it can arise both from partial degradation of  $[\text{Zr-MOP}]$  or by direct reaction with  $(\text{n-butylCp})_2\text{ZrCl}_2$  (See SI). The monomeric nature of  $[\text{n-butylCpZrPW}_{11}\text{O}_{39}]^{4-}$  polyoxometalate found in the structure of  $[\text{Zr-MOP}][\text{ZrCp}_W\text{-POM}]$  is a consequence of the *n*-butylCp capping ligand.

$^1\text{H}$  and  $^{31}\text{P}$  NMR spectroscopy in  $\text{DMSO-}d_6$  confirm the formation and stability of the hybrid salts, showing the characteristic  $^1\text{H}$  NMR signals of the  $[\text{((n-butylCpZr)}_3(\text{O}_4\text{H}_{3.75}))_4(\text{benzene-1,4-dicarboxylate})_6]^{6+}$  cages and the  $^{31}\text{P}$  NMR signals for  $[\text{PMo}_{12}\text{O}_{40}]^{3-}$  and  $[\text{n-butylCpZrPW}_{11}\text{O}_{39}]^{4-}$  polyoxometalates (Figures S3–S5, Supporting Information).

$\text{N}_2$  (77 K) and  $\text{CO}_2$  (273 K) adsorption isotherms have been measured to assess the accessibility of pore pockets in the hybrid

salts (Figure S7, Supporting Information). [Zr-MOP][ZrCp\_W-POM] is not porous to N<sub>2</sub> molecules while [Zr-MOP][Mo-POM] salt exhibits a moderate porosity (S BET of 100.9 m<sup>2</sup> g<sup>-1</sup>) related to inter ion 5–6 Å channels created after removal of the DMA solvation molecules. Noteworthy, both hybrid salts are porous to CO<sub>2</sub> with 0.6 and 1.1 mmol g<sup>-1</sup> being adsorbed at 1 bar and 273 K for [Zr-MOP][Mo-POM] and [Zr-MOP][ZrCp\_W-POM], respectively. This result agrees with the higher kinetic energy of this probe molecule allowing its access to tetrahedral cage voids (490 Å<sup>3</sup>) through ≈4.0 Å triangular windows.

## 2.1. Thermochemistry

The electronic and redox properties for [Zr-MOP][Mo-POM] and [Zr-MOP][ZrCp\_W-POM] have been studied by means of diffuse reflectance, cyclic voltammetry, and computational chemistry (Figure 2; Figures S8–S10 and Tables S2 and S3, Supporting Information). Cyclic voltammetry studies, in DMA solution, evidence the similar behavior of the hybrid salts and the independent components. [Zr-MOP] shows oxidation and reduction features at ≈0.95 and –2.3 V versus H<sub>2</sub>/2H<sup>+</sup>, corresponding to organic ligand-centered and node-centered redox processes, respectively.

W/Mo-POMs display reduction waves at milder potentials close to –0.4 V versus H<sub>2</sub>/2H<sup>+</sup> corresponding to M<sup>6+</sup> to M<sup>5+</sup> reduction. For [ZrCp\_W-POM], a redox wave with an onset at ≈0.95 V versus H<sub>2</sub>/2H<sup>+</sup>, corresponding to the probable Cp residue oxidation, is observed. Analysis of the hybrid salts, in DMA solution, results in the presence of similar redox features (Figure 2a; Figure S8, Supporting Information). However, upon cycling, the POM-related features in [Zr-MOP][Mo-POM] become highly irreversible indicative of poor electrochemical stability (Figure S8, Supporting Information). In contrast, [Zr-MOP][ZrCp\_W-POM] retains the main redox features upon cycling as evidence of its enhanced stability under highly reductive conditions (Figure 2a). In addition, a small shift is observed in the case of the W-POM redox features consistent with the substitution of a W by a Zr atom in the heterometallic [ZrCp\_W-POM] structure.

The Tauc plot analysis of the electronic spectra has allowed us to estimate a bandgap of 3.25 eV for [Zr-MOP][ZrCp\_W-POM] hybrid salt (Figure 2b). Similarly to cyclic voltammetry studies, the observed bandgap is averaged from its individual components (Figure S9, Supporting Information).<sup>19]</sup>

Time-dependent-Density Functional Theory (TD-DFT) using a cluster model of the Zr-MOP polyhedra limited to one Zr<sub>3</sub>O-node surrounded by three n-butylCp capping ligands and three benzoate ligands reveals an electronic transition located at 371 nm, in good agreement with the UV–vis spectra of [Zr-MOP] cage. Analysis of the involved molecular orbitals supports a charge transfer process from Cp-centered π orbitals to a largely delocalized molecular orbital involving both Zr-node but also terephthalate linkers (Figure 2c; Figure S10b, Supporting Information). Similarly, the computational calculation for the [ZrCp\_W-POM] fragment shows the most probable absorption band located at 363 nm. Analysis of the molecular orbitals involved in this transition agrees with a charge transfer process from Cp-centered π orbitals to a largely delocalized molecular or-

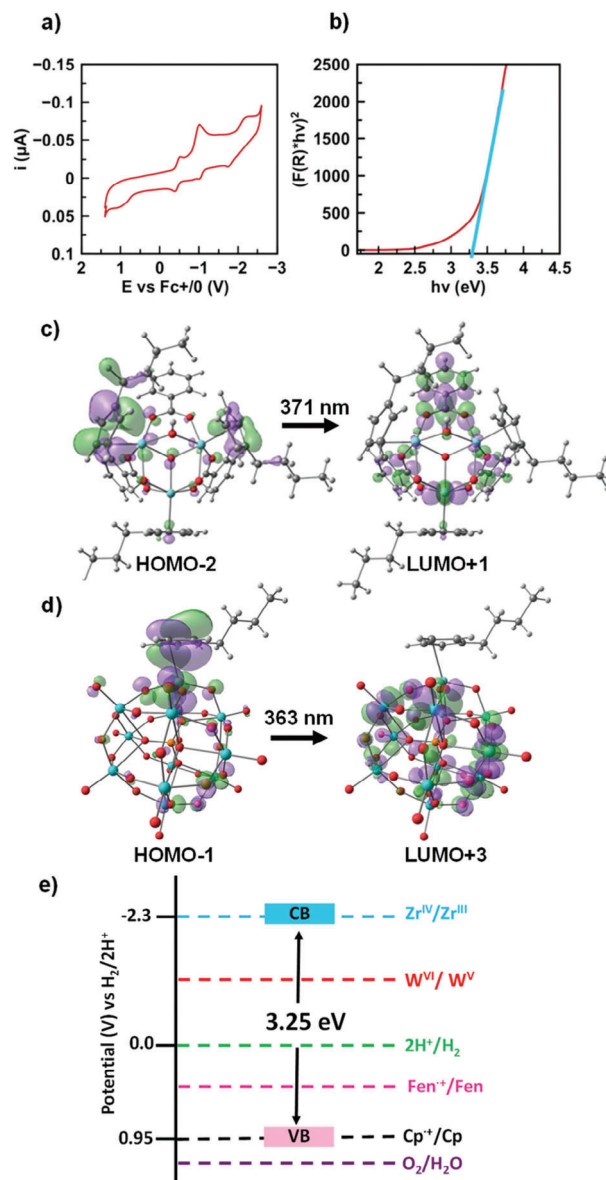


**Figure 2.** Summary of photo and electrochemical properties of [Zr-MOP][ZrCp\_W-POM] hybrid salt: a) cyclic voltammetry and b) optical bandgap from Tauc plot analysis; molecular orbitals involved in the calculated charge transfer transition bands for c) [Zr-MOP] and d) [ZrCp\_W-POM] salt fragments; e) proposed band structure for [Zr-MOP][ZrCp\_W-POM] hybrid salt.

bital involving the W atoms in the POM residue (Figure 2d; Figure S10a, Supporting Information). We thus associate these charge transfer processes in [Zr-MOP][ZrCp\_W-POM] to the generation of a charge-separated state with a potential oxidizing character.

On the basis of electronic spectra, cyclic voltammetry, and computational results for the [Zr-MOP][ZrCp\_W-POM] salt and its components we have been able to propose a band structure (Figure 2e). The valence band is located at 0.95 V versus H<sub>2</sub>/2H<sup>+</sup> and is attributed to the organic residues (cyclopentadienyl) oxidation of the [Zr-MOP] cages and [ZrCp\_W-POM]. The

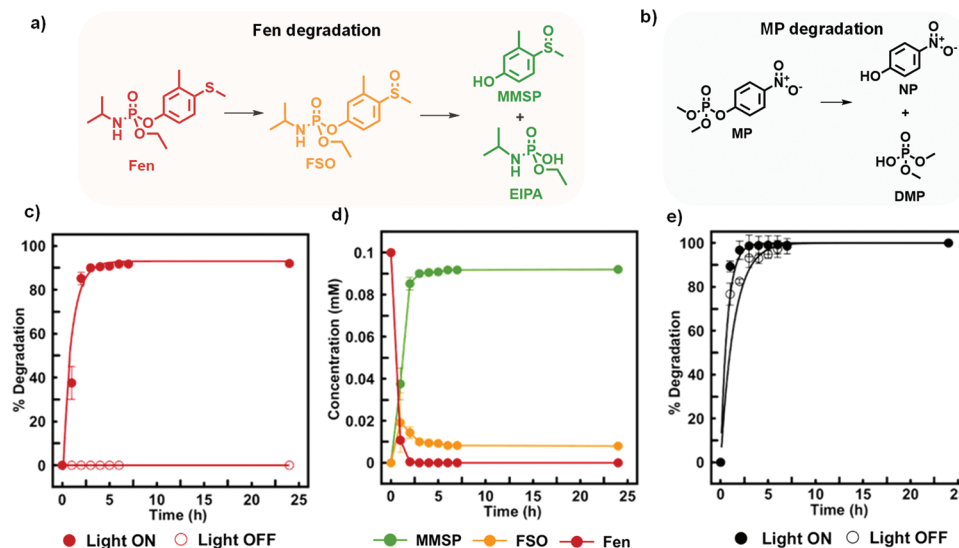


**Figure 3.** Catalytic detoxification of OPs by [Zr-MOP][ZrCp\_W-POM]: a) photooxidative-hydrolytic and b) hydrolytic degradation pathways for Fen and MP pollutants, respectively; c) photooxidative-hydrolytic degradation of Fen pollutant with light on (full circles) and in the dark (open circles); d) component variation along the photodegradation reaction pathway of Fen; e) hydrolytic degradation of MP with light on (full circles) and in the dark (open circles). Experimental conditions: 0.1 M OP unbuffered aqueous solutions (10 mL) under 390 nm light irradiation ( $400 \text{ mW cm}^{-2}$ ) in the presence of [Zr-MOP][ZrCp\_W-POM] (0.5  $\mu\text{mol}$ ).

conduction band located at  $-2.3 \text{ V}$  versus  $\text{H}_2/2\text{H}^+$  is attributed to the one-electron reduction of the (n-butylCpZr)<sub>3</sub> nodes giving rise to a bandgap of 3.25 eV (Figure 2e). These features give rise to an efficient behavior in photooxidation processes as exemplified by fenamiphos photo-driven detoxification.

## 2.2. Tandem Photooxidative and Hydrolytic Degradation of Persistent Fenamiphos

Once we proved the structural and thermochemical properties of [Zr-MOP][ZrCp\_W-POM] and [Zr-MOP][Mo-POM] hybrid salts, we explored the behavior of these systems as heterogeneous catalysts for the degradation of highly persistent fenamiphos (Fen) pollutant in unbuffered aqueous solutions. On the basis of the band structure of [Zr-MOP][ZrCp\_W-POM], with a bandgap of 3.25 eV (see above), we have selected a 390 nm ( $3.2 \text{ eV}$ ) lamp with a 50 W power ( $400 \text{ mW cm}^{-2}$ ) as a suitable source to photoactivate our materials.

The results show that [Zr-MOP][ZrCp\_W-POM] hybrid salt (0.5  $\mu\text{mol}$ ), under light irradiation, is able to readily degrade an unbuffered Fen aqueous solution (0.1 mM, 10 mL) into 3-methyl-4-(methylsulfinyl)phenol (MMSP) ( $k = 1.02 \text{ h}^{-1}$ ,  $t_{1/2} = 0.7 \text{ h}$ , turn over number (TON) = 1.86, 1:2 salt to Fen ratio) (Figure 3, Table 1). Pollutant degradation involves a two-step process consisting of the sequential photo-driven oxidation of toxic Fen ( $\text{LD}_{50}$  oral rat of  $2.5 \text{ mg kg}^{-1}$ ) to still toxic fenamiphos sulfoxide (FSO,  $0.5 \text{ V}$  vs  $\text{H}_2/2\text{H}^+$ ,  $\text{LD}_{50}$  oral rat of  $10 \text{ mg kg}^{-1}$ ) and subsequent hydrolytic degradation into low toxicity MMSP ( $\text{LD}_{50}$  oral rat of  $1,420 \text{ mg kg}^{-1}$ ) and phosphate derivatives, as found by GC-MS and HPLC UV-vis measurements (Figure 3c,d; Figure S11, Supporting Information). A hot filtration test is indicative of the heterogeneity of the photocatalytic reaction (Table S3, Supporting Information). In the absence of the salt catalyst, Fen is highly sta-

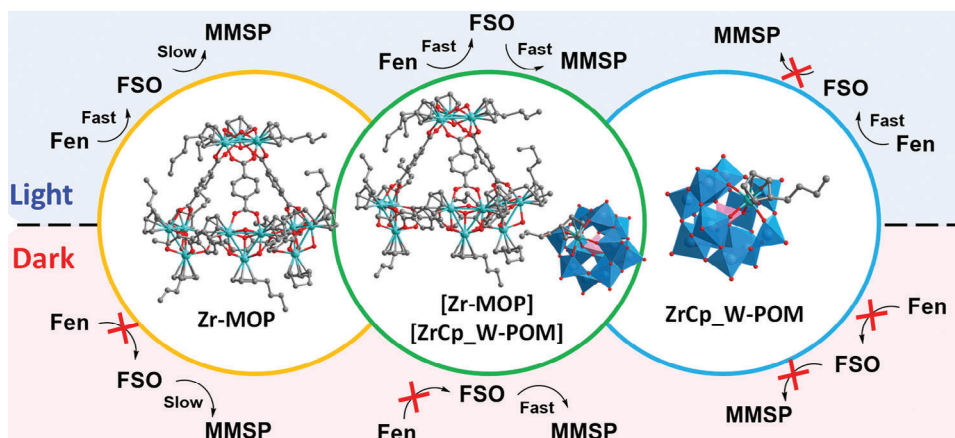
**Table 1.** Kinetics and efficiency for detoxification of 0.1 M unbuffered aqueous solutions (10 mL) of Fen, FSO and MP organophosphates to MMSP, MMSF and *p*-nitrophenol, respectively, by [Zr-MOP][ZrCp\_W-POM] (0.5  $\mu\text{mol}$ ) hybrid salt catalyst under light irradiation (390 nm) and in the dark. Catalyst to Organophosphate ratio 1:2.

Substrate	Light on			Light off		
	$k$ [ $\text{h}^{-1}$ ]	$t_{1/2}$ [h]	yield [%] <sup>a)</sup>	$k$ [ $\text{h}^{-1}$ ]	$t_{1/2}$ [h]	yield [%] <sup>a)</sup>
Fen	1.02	0.7	93	–	–	–
FSO	0.82	0.8	100	0.23	3.1	90
MP	1.41	0.5	100	0.7	1.0	100

<sup>a)</sup> Reaction yield after 24 h.

ble under light irradiation with no appreciable degradation over 24 h control tests (see Table S10, Supporting Information). In the dark, the salt catalyst is inactive for Fen degradation (Figure 3c). By contrast, FSO is also hydrolyzed in the dark ( $k = 0.23 \text{ h}^{-1}$ ,  $t_{1/2} = 3.1 \text{ h}$ , TON = 2) highlighting that photooxidation is the key step for Fen detoxification (Figure S12, Supporting Information; Table 1).

Noteworthy, the performance of the individual components [Zr-MOP] and [ZrCp\_W-POM] for Fen hydrolytic photodegradation is poorer than the hybrid salt (Scheme 2; Figure S13, Supporting Information). [ZrCp\_W-POM] gives only rise to the very rapid photooxidation to FSO ( $k = 1.26 \text{ h}^{-1}$ ,  $t_{1/2} = 0.6 \text{ h}$ ) with the quantitative conversion being achieved after 2.5 h (TON = 2, Figure S14, Supporting Information). [Zr-MOP] not only photooxidizes Fen to FSO but also performs the subsequent hydrolysis of FSO to MMSP, although exhibiting a slower hydrolysis rate than [Zr-MOP][ZrCp\_W-POM]. Specifically, light irradiation of a Fen solution for 2 h, in the presence of [Zr-MOP], gives rise to a mixture of 70% photooxidized FSO and 30% hydrolyzed MMSP.



**Scheme 2.** Summary of the degradation reactivity promoted by the [Zr-MOP][ZrCp\_W-POM] hybrid salt and its components ([Zr-MOP] cage and [ZrCp\_W-POM] polyoxometalate) toward Fen pollutant under light irradiation and in the dark.

After 24 h, the reaction mixture evolves to 36.5% of photooxidized intermediate FSO and 63.5% of the fully degraded MMSP (Figure S14, Supporting Information). ICP and NMR analysis of [ZrCp\_W-POM], after the photodegradation studies, indicates the leaching of ZrCp, W and P to the supernatant solution, a potential reason for its poorer performance. By contrast, the hybrid salt is chemically stable under similar conditions (Figures S15–S17 and Table S5, Supporting Information). These results, summarized in Scheme 2, highlight the importance of the two-step reaction pathway (photooxidation + hydrolysis) and the synergistic behavior of the hybrid salt components for the full degradation of Fen to MMSP. Using [Zr-MOP][Mo-POM] instead fails to yield the full degradation process of Fen, progressing to the FSO oxidation step only. This is consistent with the poorer [Zr-MOP][Mo-POM] stability with irreversible voltammograms and leaching of Zr and Mo ions from the salt structure after photoactivation (Figure S8 and Table S5, Supporting Information). This result is in line with general observations of lower stability of Mo-POM in comparison to W-POM.<sup>[20]</sup> Moreover, Fen degradation under light irradiation, in the presence of benchmark materials such as TiO<sub>2</sub>,<sup>[21]</sup> UiO-66, and NU-1000 Zr-MOFs systems and Keggin phosphotungstenate H<sub>3</sub>[PW<sub>12</sub>O<sub>40</sub>] leads to either toxic FSO photooxidation intermediate or to a lower detoxification efficiency to MMSP than the hybrid salt (See Figure S18, Supporting Information).

We further interrogated the mechanism of the oxidation process of Fen by [Zr-MOP][ZrCp\_W-POM]. Previous work has leveraged the photocatalytic generation of highly reactive oxygen-based species, such as OH·, for the degradation of toxic molecules.<sup>[22]</sup> The band structure of our system does not allow the generation of such species (2.8 V vs H<sub>2</sub>/2H<sup>+</sup>, Figure 2d). Indeed, performing similar photodegradation experiments in non-aqueous media and in the absence of O<sub>2</sub> gives rise to photooxidized FSO. In an aqueous solution and inert atmosphere, the photo-driven detoxification process evolves to the fully degraded MMSP (Table S6, Supporting Information). These results support the direct photooxidation of Fen by [Zr-MOP][ZrCp\_W-POM] without the need to generate highly reactive oxygen species. This has an additional benefit as it allows for a readily accessible tuning of the photoredox potentials by appropri-

ate choice of salt components to meet the needs of the oxidative degradation of the substrate.

### 2.3. Degradation of Methylparaoxon and Multicomponent Mixtures of Organophosphate Pesticides

To broaden the scope of this study we have explored the hydrolytic degradation, in unbuffered aqueous media, of the prototypical toxic OP methylparaoxon (MP) as well as multicomponent OP mixtures of Fen, FSO, and MP.

Highly toxic MP (LD<sub>50</sub> oral rat of 3.3 mg kg<sup>-1</sup>) can be converted to low toxicity *p*-nitrophenol (LD<sub>50</sub> oral rat of 667 mg kg<sup>-1</sup>) and dimethylphosphate (LD<sub>50</sub> oral rat of 3.280 mg kg<sup>-1</sup>) (Figure 3b). The results show that [Zr-MOP][ZrCp\_W-POM] hybrid salt is highly active for MP hydrolysis (1:2 hybrid salt to MP ratio), in unbuffered aqueous solutions, both under light irradiation ( $k = 1.41 \text{ h}^{-1}$ ,  $t_{1/2} = 0.49 \text{ h}$ , TON = 2) and in the dark ( $k = 0.70 \text{ h}^{-1}$ ,  $t_{1/2} = 0.98 \text{ h}$ , TON = 2) (Figure 3e, Table 1). [Zr-MOP] shows a similar MP hydrolytic performance than the hybrid salt both under light irradiation ( $k = 1.47 \text{ h}^{-1}$ ,  $t_{1/2} = 0.48 \text{ h}$ , TON = 2), and in the dark ( $k = 0.59 \text{ h}^{-1}$ ,  $t_{1/2} = 1.17 \text{ h}$ , TON = 2). By contrast, [ZrCp\_W-POM] shows a poorer hydrolytic activity reaching 27.5% of MP hydrolysis after 24 h (Figure S19 and Table S7, Supporting Information). These results point that the hydrolytic activity for MP detoxification is centered at the [Zr-MOP] cage as reported previously for related [(CpZr)<sub>3</sub>(O<sub>4</sub>H<sub>3,75</sub>)<sub>4</sub>(benzene-1,4-dicarboxylate)<sub>6</sub>]Cl<sub>6</sub>.<sup>[14]</sup>

In order to understand why [Zr-MOP][ZrCp\_W-POM] hybrid salt is not able to hydrolyze Fen in the dark, while FSO and MP are hydrolyzed, we have studied the acid-base properties of the phenolate residues in the OP molecular structures (Figure S20 and Table S8, Supporting Information). The acidity of 3-methyl-4-(methylthio)phenol (pKa = 10.11) increases significantly after sulfur atom oxidation to 3-methyl-4-(methylsulfinyl)phenol (pKa 7.71). Noteworthy, the later value is very similar to *p*-nitrophenol pKa value of 7.16. The decreased basicity of phenolate residues in the studied OP determines their hydrolytic stability (persistence), under dark conditions, with the hydrolytic degradation rates following the trend  $k_{\text{Fen}} \ll k_{\text{FSO}} < k_{\text{MP}}$  (Table 1) correlating

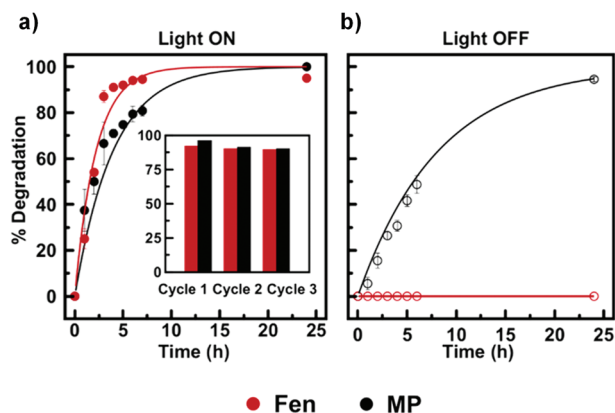


**Figure 4.** a) Simultaneous degradation profiles for equimolecular 0.05 m unbuffered aqueous solutions (10 mL) of Fen (red circles) and MP (black circles) under 390 nm light irradiation in the presence of [Zr-MOP][ZrCp-W-POM] (0.5  $\mu\text{mol}$ ): the inset in (a) shows three catalyst recyclability tests; b) Degradation profiles for Fen (open red circles) and MP (open black circles) mixtures in the dark.

the reverse values of  $pK_a$ s. Under light irradiation, the degradation kinetics follows the Fen  $\sim$  FSO  $<$  MP trend (Table 1) which is indicative of the key role of the photooxidation step for Fen degradation.

Aiming to approach real environmental conditions we have investigated the response of [Zr-MOP][ZrCp-W-POM] hybrid salt to multicomponent pesticide unbuffered aqueous solutions containing Fen, FSO, and MP. [Zr-MOP][ZrCp-W-POM] hybrid salt (0.5  $\mu\text{mol}$ ), under 390 nm irradiation, is able to degrade an equimolecular unbuffered aqueous solution (0.05 mM, 10 mL H<sub>2</sub>O) of Fen ( $k = 0.46 \text{ h}^{-1}$ ,  $t_{1/2} = 1.52 \text{ h}$ ) and MP ( $k = 0.25 \text{ h}^{-1}$ ,  $t_{1/2} = 2.7 \text{ h}$ ) pollutants into low toxicity 3-methyl-4-(methylsulfinyl)phenol and *p*-nitrophenol, respectively (Figure 4a; Figure S21 and Table S9, Supporting Information). The significant slowdown of the MP degradation rate (82%) in the presence of Fen might indicate a competitive interaction of Fen over MP with the catalyst surface. Noteworthy, this catalytic detoxification process can be repeated for three consecutive cycles (inset in Figure 4a) increasing the TON of the catalyst to 6. This result further proves the enhanced stability of the salt over its individual components. A similar experiment, in the dark, indicates that the detoxification reaction proceeds only for hydrolytic detoxification of MP ( $k = 0.12 \text{ h}^{-1}$ ,  $t_{1/2} = 5.6 \text{ h}$ ) (Figure 4b; Table S9, Supporting Information) which is in line with the single component studies (see above). Next, we tested the hydrolytic activity of the hybrid salt toward an equimolecular mixture of FSO and MP (Figures S22 and S23, Supporting Information). Under 390 nm light irradiation both FSO ( $k = 0.69 \text{ h}^{-1}$ ,  $t_{1/2} = 1.0 \text{ h}$ ) and MP ( $k = 0.24 \text{ h}^{-1}$ ,  $t_{1/2} = 2.98 \text{ h}$ ) are hydrolyzed (Table S9, Supporting Information). Noteworthy, Fen and FSO degradation follow a similar kinetic profile. This suggests that hydrolysis is the rate-determining step for the photo-promoted degradation process.

### 3. Conclusions

We have formed a functional [Zr-MOP][ZrCp-W-POM] hybrid salt exhibiting a photoactivated charge-separated state with oxidative and hydrolytic properties. This material is highly active in

the detoxification of organophosphorus pesticides in unbuffered aqueous solutions. While persistent Fen is hard to hydrolyze, we have a tandem photooxidation/hydrolytic process catalyzed by [Zr-MOP][ZrCp-W-POM] to fully detoxify this persistent pollutant. Noteworthy, this approach can be extended to the detoxification of OP mixtures as exemplified by simultaneous degradation of Fen, FSO, and MP, under environmentally relevant conditions. Our findings underscore the utility of incorporating Zr-MOP and POM constituents into functional [Zr-MOP][POM] hybrid salts to tune its photochemical, redox, acid-base, and stability features, leading to clear synergies between the individual components.

### Supporting Information

Supporting Information is available from the Wiley Online Library or from the author.

### Acknowledgements

C.P.-B. and R.V. contributed equally to this work. The authors are grateful to Spanish MCIN/AEI/10.13039/501100011033 (Projects: PID2020-113608RB-I00 and TED2021-129886B-C41) and FEDER Junta de Andalucía – Conserjería de Universidad, Innovación e Investigación (Project C-EXP-056-UGR-23). CP acknowledges Spanish MCIN for a predoctoral fellowship PRE2021-099867. P.G.-B. thanks the grant RYC2021-031249-I funded by MICIU/AEI/10.13039/501100011033 and by “European Union NextGenerationEU/PRTR”. TJB thanks Universidad de Granada for the Visiting Scholar program. N.M.P. thanks the La Caixa Foundation for a Postdoctoral Junior Leader–Retaining Fellowship (ID 100010434, fellowship code LCF/BQ/PR20/11770014), the Generalitat Valenciana for the projects (MFA/2022/026 and SEJIGENT/2021/059), and the Spanish government (project PID2020-118117RB-I00). The authors thank Centro de Servicios de Informática y Redes de Comunicaciones (CSIRC), Universidad de Granada, for providing the computing time.

### Conflict of Interest

The authors declare no conflict of interest.

### Data Availability Statement

The data that support the findings of this study are available from the corresponding author upon reasonable request.

### Keywords

DFT calculations, heterogeneous catalysis, molecular cage, organophosphorous, photoredox catalysis

Received: April 4, 2024  
Revised: May 26, 2024  
Published online:

- [1] W. Boedeker, M. Watts, P. Clausing, E. Marquez, *BMC Public Health* **2020**, *20*, 1875.
- [2] R. A. Tessema, K. Nagy, B. Ádám, *Front. Public Heal* **2022**, *10*, 1.
- [3] *Interim Reregistration Eligibility Decision (IRED) for fenamiphos*, US Protection Agency Environmental, Washington, D.C., **2002**.

- [4] M. K. Kinnan, W. R. Creasy, L. B. Fullmer, H. L. Schreuder-Gibson, M. Nyman, *Eur. J. Inorg. Chem.* **2014**, 2014, 2361.
- [5] D. L. Collins-Wildman, M. Kim, K. P. Sullivan, A. M. Plonka, A. I. Frenkel, D. G. Musaev, C. L. Hill, *ACS Catal.* **2018**, *8*, 7068.
- [6] E. Tanuhadi, E. Al-Sayed, A. Roller, H. Čipčić-Paljetak, D. Verbanac, A. Rempel, *Inorg. Chem.* **2020**, *59*, 14078.
- [7] D. E. Salazar Marciano, N. D. Savić, K. Declerck, S. A. M. Abdelhameed, T. N. Parac-Vogt, *Chem. Soc. Rev.* **2023**, *53*, 84.
- [8] S. Vanhaecht, G. Absillis, T. N. Parac-Vogt, *Dalt. Trans.* **2012**, *41*, 10028.
- [9] J. J. Walsh, A. M. Bond, R. J. Forster, T. E. Keyes, *Coord. Chem. Rev.* **2016**, *306*, 217.
- [10] L. A. M. Mahmoud, R. A. Dos Reis, X. Chen, V. P. Ting, S. Nayak, *ACS Omega* **2022**, *7*, 45910.
- [11] J. Tang, P. Li, T. Islamoglu, S. Li, X. Zhang, F. A. Son, Z. Chen, M. R. Mian, S. J. Lee, J. Wu, O. K. Farha, *Cell Reports Phys. Sci.* **2021**, *2*, 100612.
- [12] L. González, F. J. Carmona, N. M. Padial, J. A. R. Navarro, E. Barea, C. R. Maldonado, *Mater. Today Chem.* **2021**, *22*, 100596.
- [13] P. Delgado, J. D. Martin-Romera, C. Perona, R. Vismara, S. Galli, C. R. Maldonado, F. J. Carmona, N. M. Padial, J. A. R. Navarro, *ACS Appl. Mater. Interfaces* **2022**, *14*, 26501
- [14] K. Kiaei, K. Brunson, A. Gładysiak, K. Smith, K. Hunter, A. Thomas, D. Radke, T. Zuehlsdorff, K. C. Stylianou, *J. Mater. Chem. A* **2023**, *11*, 14265.
- [15] M. C. De Koning, M. Van Grol, T. Breijaert, *Inorg. Chem.* **2017**, *56*, 11804.
- [16] F. Liu, I. Rincón, H. G. Baldoví, A. Dhakshinamoorthy, P. Horcajada, S. Rojas, S. Navalón, A. Fateeva, *Inorg. Chem. Front.* **2024**, *11*, 2212.
- [17] B. L. Ouay, H. Yoshino, K. Sasaki, Y. Ohtsubo, R. Ohtani, M. Ohba, *Chem. Commun.* **2021**, *57*, 5187.
- [18] K. Nomiyama, Y. Saku, S. Yamada, W. Takahashi, H. Sekiya, A. Shinohara, M. Ishimaru, Y. Sakai, *Dalt. Trans.* **2009**, *2*, 5504.
- [19] P. Makuła, M. Pacia, W. Macyk, *J. Phys. Chem. Lett.* **2018**, *9*, 6814.
- [20] M. Laurans, M. Mattera, R. Salles, L. K'Bidi, P. Gouzerh, S. Renaudineau, F. Volatron, G. Guillemot, S. Blanchard, G. Izzet, A. Solé-Daura, J. M. Poblet, A. Proust, *Inorg. Chem.* **2022**, *61*, 7700.
- [21] A. El Yadini, H. Saufi, P. S. M. Dunlop, J. A. Byrne, M. El Azzouzi, S. El Hajjaji, *J. Catal.* **2014**, *2014*, 413693.
- [22] L. Gan, M. T. Nord, J. M. Lessard, N. Q. Tufts, A. Chidambaram, M. E. Light, H. Huang, E. Solano, J. Fraile, F. Suárez-García, C. Viñas, F. Teixidor, K. C. Stylianou, J. G. Planas, *J. Am. Chem. Soc.* **2023**, *145*, 13730.